

# Non-linear magnetohydrodynamic hybrid simulations of the stability in tokamaks



**Pablo Oyola Domínguez**

Departamento de Física Atómica, Molecular y Nuclear

Universidad de Sevilla

Supervisor: Dr. Manuel García Muñoz and Dr. Eleonora Viezzer

Advisor: Javier Gonzalez-Martin

*Grado en Física*



## Abstract

Plasma physics plays a fundamental role in fusion technology research. However, the main equations governing the plasma dynamics, Navier-Stokes coupled with Maxwell equations, have challenges such as non-linearity and multiple coupling among all the evolving properties. Thus, any analytical study has been reduced to linearized models, which can not properly reproduce the plasma behavior. These simple analytical models cannot fully reproduce an important and current drawback in fusion devices, i.e., plasma instabilities in tokamaks. Instabilities represent a non-negligible contribution to the loss of plasma confinement. Consequently, they limit the fusion energy release and also represent a source of material damage.

Understanding, predicting and, eventually, mitigating these instabilities is an open research line within the plasma and fusion community. Accordingly, these instability studies should be carried out from both experimental and theoretical points of view, obtaining, in the theoretical approach, analytical results from equations and finally, solving numerically the plasma dynamics. This approach is followed in this work in order to study one particular type of instability, *Toroidal Alfvén Eigenmode*, TAE, giving a physical and mathematical background of its origin and carrying out several numerical simulations of the plasma dynamics. To study these instabilities, a realistic geometry has been developed during this work. The properties of the simulated losses are studied and correlated with the detection of the TAE instabilities inside the plasma.



# Table of contents

<b>1</b>	<b>Introduction</b>	<b>1</b>
<b>2</b>	<b>Plasma physics</b>	<b>5</b>
2.1	The fluid model . . . . .	5
2.2	Tokamak . . . . .	8
2.2.1	Drift-kinetic theory . . . . .	8
2.2.2	The magnetic dipole moment . . . . .	10
2.2.3	The need for a tokamak . . . . .	11
2.3	Toroidal Alfvén Eigenmodes . . . . .	14
<b>3</b>	<b>The physical framework: MEGA</b>	<b>19</b>
3.1	The physical background: Hazeltine-Meiss model . . . . .	20
3.2	Initial conditions . . . . .	23
3.3	Fast-ions . . . . .	25
3.4	The simulation domain . . . . .	27
<b>4</b>	<b>MEGA wall</b>	<b>29</b>
4.1	Numerical background . . . . .	29
4.2	A realistic 3D wall for MEGA . . . . .	30
4.3	Simulations and discussion . . . . .	32
<b>5</b>	<b>Conclusions and future work</b>	<b>39</b>
	<b>Nomenclature</b>	<b>41</b>

<b>References</b>	<b>43</b>
<b>Appendix A Theoretical plasma physics</b>	<b>45</b>
A.1 Eigenvalue equation for MHD instabilities . . . . .	45
A.2 Hazeltine-Meiss model: viscosity and energetic particles . . . . .	46
A.3 Grad-Shafranov equation . . . . .	49

# Chapter 1

## Introduction

The recent evolution of new technologies has led the human beings to be more and more dependent on energy. Nowadays, this increasing need of electric power is leading the world to the research of new sources of energy, that can both supply enough power to support these new technologies and completely substitute the non-renewable power sources. One of the main concerns of this research is the constant increment of emission of gases which are producing the green-house effect and would definitively lead the world to a non-return point.

One of the most promising fields in order to solve such important issues was found when investigating the physics of the stars: how can stars produce such amount of energy? The astronomers and the astrophysicists studied these celestial objects for years until they found the answer: gravitational nuclear fusion. Nuclear fusion is a well-established process<sup>1</sup>: in a Sun-like star, the main source of power is the *p-p chain* in which 4 protons fuse (by means of both nuclear interactions) to produce an  $\alpha$  particle. This mechanism seems to be adequate for the problem stated: the fuel is hydrogen and the residuals are helium particles, in contrast to those of non-renewable sources.

Nonetheless, this first approach of exactly reproducing the mechanism of the Sun on Earth is not the best one. First of all,  $p^+ + p^+ \rightarrow {}^2H + e^- + \bar{\nu}_e$  process is dominated

---

<sup>1</sup>There are, however, remaining open questions, but the main mechanism is well understood.

by the weak force and its half-life is of the order of  $10^{10}$  years. Therefore, it is quite unlikely to happen in a hypothetical reactor. The large densities, temperatures and the strength of the gravitational force in the Sun's core are the catalyst of such an unlikely process. This issue then led the fusion researchers to look for a new point of view.

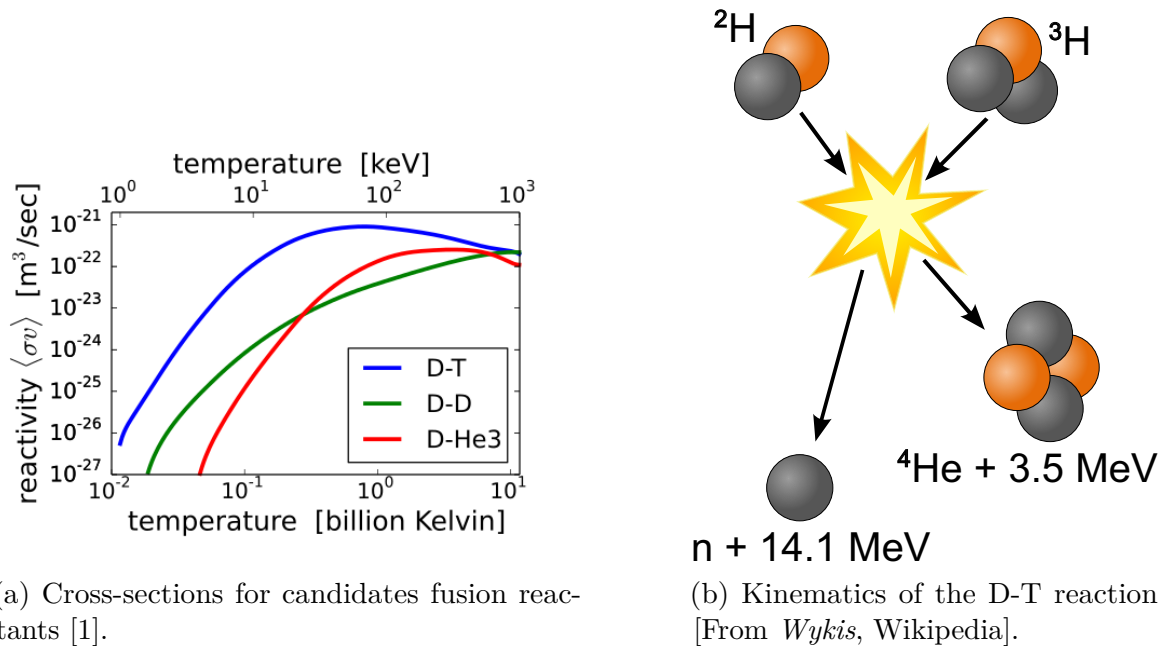


Fig. 1.1 Candidate nuclear reactions for a fusion device: cross-sections and kinematics of the D-T reaction.

The best candidate for nuclear fusion is the D-T reaction: as shown in figure 1.1a, it has a large cross-section over a wide energy range. Apart from that, from this figure one can also conclude that D-T has also the minimum temperature for the maximum cross-section. Dealing with this kind of reactions always implies high temperatures (billions of degrees), so it is necessary to stand against a new drawback. There is no material that can support and control this high temperature without melting: increasing the temperature, matter reaches the fourth state, the plasma state.

This plasma state is precisely the motivation of the present project, and in particular, study the instabilities that produce a degradation in the plasma confinement. In the second chapter, the fundamentals of plasma physics are presented, briefly describing the main model of plasma physics, magnetohydrodynamics (MHD) and its implications

for modeling and instabilities in a reactor. The main issue the MHD model carries is the complexity and non-linearity of the equations, so numerical methods are required. The third chapter is dedicated to a description of a numerical approach in order to solve this model, MEGA [2], which includes all this complexity in the model and also introduces the effect of energetic particles, appearing within the plasma (the fusion-born  $\alpha$  particles among many others). This simulation code represents an important approach to study the instabilities induced either by the MHD-plasma, energetic particles or their coupling. Up to now, the resolution of the model equations has been carried out without taking into account a realistic geometry for the integration domain.

The object of this work is, therefore, to study the inclusion of a realistic 3D wall in the simulation code. In the fourth chapter the implementation is discussed and the results obtained from several simulations are presented both for benchmark studies and data analysis. A synthetic diagnostic for the fast-ion loss detector (FILD)[3–5], as a part of the realistic wall, has been implemented enabling the analysis of the velocity-space of the simulated losses, which will be compared to experimental data from ASDEX Upgrade experiment<sup>2</sup>.

---

<sup>2</sup>Max Planck Institute for Plasma Physics, Garching



# Chapter 2

## Plasma physics

In this chapter, the fundamentals of plasma physics are briefly introduced. First of all, the fluid model of the plasma and the typical motion of particles within a general magnetic field are discussed. From those concepts, the tokamak principles are introduced, describing its main characteristics. Finally, the issue of the instabilities is presented along with a more detailed discussion about one important kind of instabilities, which is the motivation of the present work.

### 2.1 Statistical description of a plasma: the fluid model

The plasma state can be characterized by two properties:

- **Quasi-neutrality:** despite the fact that the plasma is composed by charged particles, it can be shown [6] that if the characteristic length of the system is much larger than the Debye length,  $\lambda_D$ , the plasma can be considered as an 'almost' neutral system:

$$\lambda_D = \sqrt{\frac{\epsilon_0 K_B T_e}{e^2 n_0}} \quad \text{where } k_B T_e \text{ is the electron temperature, given in energy units.}$$

- **Collective effects:** the most important interactions in a plasma are produced by the plasma as a collective system rather than by one-to-one interactions. This condition is met if in a Debye volume ( $\lambda_D^3$ ) there are enough particles.

For an appropriate description of the plasma, the fact that in a plasma ions and electrons are separated needs to be taken into account<sup>1</sup>. This leads to interactions between the charged particles and the electromagnetic fields (either externally applied, or due to Coulomb collisions). Like in any many-body problem, the statistical approach has to be used, obtaining the Boltzmann equation for the distribution function<sup>2</sup>:

$$\frac{\partial f_s}{\partial t} + \vec{v} \cdot \vec{\nabla}_r f_s + \frac{q_s}{m_s} [\vec{E} + \vec{v} \times \vec{B}] \cdot \vec{\nabla}_v f_s = \left( \frac{\partial f_s}{\partial t} \right)_C \quad (2.1)$$

Here  $\vec{E}$  and  $\vec{B}$  are the long-range electric and magnetic fields, and the equation determines the evolution of the distribution function of a specie  $s$ , whose mass and charge are  $m_s$  and  $q_s$ , having a velocity  $\vec{v}$ . The short-range interactions, i.e., the Coulomb collisions between particles are grouped into the **collision operation**,  $\left( \frac{\partial f_s}{\partial t} \right)_C$ . From this equation the Particle-in-Cell (PIC) method is derived, which will be introduced in Chapter 3.

The general solution of (2.1) is computationally quite expensive, so further simplifications are needed. It is possible to represent the plasma by three moments of the Boltzmann equation, i.e., the plasma can be described as a fluid. This will eventually lead to the Navier-Stokes equations coupled with the Maxwell equations, since the fluid consists on charged particles. There are different levels of approximation, depending on how many interacting fluids are considered. In the present work, the one-fluid approach is used [6]. The plasma is characterized by its density (zero-th moment), the linear momentum (the first moment) and the energy (the second moment), whose evolution in time can be obtained by integrating (2.1) in the velocity-space:

<sup>1</sup>The typical temperatures in the core of fusion plasmas are  $k_B T_e \approx 10$  keV, whilst the typical ionization energies are of the order of 10 eV.

<sup>2</sup>Since a plasma can be considered as a Hamiltonian system, Liouville theorem applies.

$$\frac{\partial \rho}{\partial t} + \vec{\nabla} \cdot (\rho \vec{v}) = 0 \quad (2.2)$$

$$\rho \frac{d\vec{v}}{dt} = \rho \vec{E} + \vec{J} \times \vec{B} - \vec{\nabla} \cdot \mathbf{P} \quad (2.3)$$

$$\frac{m_e}{n_e e^2} \frac{d\vec{J}}{dt} = \vec{E} + \vec{v} \times \vec{B} - \frac{1}{en} \vec{\nabla} \cdot \mathbf{P} - \eta \vec{J} \quad (2.4)$$

where  $\rho$  and  $\vec{v}$  are the mass density and the velocity of that fluid and  $\mathbf{P}$  is the pressure tensor. Note that this set of equations is not closed. There is need for a closure equation that relates the pressure with the rest of the parameters. For a scalar pressure, the closure can be expressed as:

$$\frac{d}{dt}(\rho p^{-\gamma}) = 0 \quad \text{Isentropic equation} \quad (2.5)$$

where  $\gamma$  is the adiabatic constant, usually taken as  $\gamma = 5/3$ , i.e., plasma is considered to behave like an ideal gas. The pressure tensor is latter discussed in Chapter 3.

The obtained equations are the **magnetohydrodynamic (MHD) model** for the plasma, which provides a good enough approximation for the plasma behavior. Here, a common concept in fluid mechanics must be introduced, the **advective derivative**:

$$\frac{d}{dt} \equiv \frac{\partial}{\partial t} + \vec{v} \cdot \vec{\nabla} \quad (2.6)$$

Further approximations can be performed in order to simplify the previous set of equations, leading to different level of approximations. In particular, the resistive model can be simply derived from (2.2)-(2.5) under three simple considerations:

1. The inertia of the electrons is negligible compared to the rest of the species, so left-hand side of equation (2.4) can be disregarded.
2. Quasi-neutrality applies and the displacement current,  $\vec{J}_D = \partial_t \epsilon_0 \vec{E}$ , can be neglected in comparison to the ohmic current.

3. The Larmor radius is small enough to remove the pressure term from equation (2.4).

With this approximations, the **resistive MHD** is described by:

$$\frac{\partial \rho_m}{\partial t} + \vec{\nabla} \cdot (\rho_m \vec{v}) = 0 \quad \text{Continuity equation} \quad (2.7)$$

$$\rho_m \frac{\partial \vec{v}}{\partial t} = \vec{J} \times \vec{B} - \vec{\nabla} p \quad \text{Momentum equation} \quad (2.8)$$

$$\vec{E} + \vec{v} \times \vec{B} = \eta \vec{J} \quad \text{Ohm's law} \quad (2.9)$$

$$\frac{d}{dt} (p \rho_m^{-\gamma}) = 0 \quad \text{Closure relation} \quad (2.10)$$

$$\vec{\nabla} \times \vec{E} = -\frac{\partial \vec{B}}{\partial t} \quad \text{Faraday's law} \quad (2.11)$$

$$\vec{\nabla} \times \vec{B} = \mu_0 \vec{J} \quad \text{Ampere's law} \quad (2.12)$$

where  $\rho_m$  is the matter density and  $\eta$  is the resistivity of the plasma.

Under the consideration of neglecting one-to-one interactions against collective effects, resistivity can also be disregarded, thus obtaining **ideal MHD**.

## 2.2 Particles drift: the need for a tokamak

### 2.2.1 Drift-kinetic theory

In the previous section, we have discussed the behavior of the plasma as a whole. Despite the collective nature of the plasma, the corrections due to particle motion can have a significant effect. In general, the plasma is usually embedded in a magnetic field, so they will follow the Lorentz force  $\vec{F}_{mag} = q\vec{v} \times \vec{B}$ . Within this magnetic field, the general motion of any charged particle is a helix following the magnetic field line (see figure 2.1) with a certain radius given by  $R_c = \frac{mv_{\perp}}{|q|B}$ , where perpendicular here refers to the orthogonality to the magnetic field.

The general motion can be decomposed into two parts: the parallel motion (parallel to the magnetic field) and the perpendicular one, which causes the gyromotion, i.e.,

the gyration around the magnetic field lines. Under a more general situation, the force includes also an electric force and other non-electromagnetic forces.

$$\vec{F} = q\vec{v} \times \vec{B} + q\vec{E} + \vec{F}_{non-em}$$

The solution of the whole equation would yield the time evolution of the mechanical state,  $(\vec{r}, \vec{v}, t)$ , of the corresponding particle. The solution of the complete equation (even numerically) can be computationally quite expensive so simplified models are required. The most descriptive approach is the **drift-kinetic model**: the guiding center of the particle is considered instead of the total motion. When the particle is submerged in a homogeneous

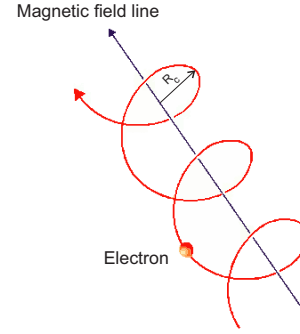


Fig. 2.1 Electron following a magnetic field line.

electromagnetic field this will follow a helical motion (as seen in 2.1). Averaging over a period of this motion (hereon, gyromotion) the perpendicular component of the acceleration,  $\dot{\vec{v}}_{\perp}$ , net value is zero, so:

$$0 = \langle m\dot{\vec{v}}_{\perp} \rangle = q(\vec{E}_{\perp} + \langle \vec{v}_{\perp} \rangle \times \vec{B}) \Rightarrow \langle \vec{v}_{\perp} \rangle = \frac{\vec{E}_{\perp} \times \vec{B}}{B^2} \quad (2.13)$$

In this case, the motion of the guiding center, in an electromagnetic field, is obtained. Consequently, the total perpendicular velocity can be expressed as two terms, the drift velocity ( $\langle \vec{v}_{\perp} \rangle$ ) plus a certain perturbation ( $\vec{v}'_{\perp}$ ).

$$\vec{v}_{\perp} = \langle \vec{v}_{\perp} \rangle + \vec{v}'_{\perp}$$

$$m \frac{d(\langle \vec{v}_{\perp} \rangle + \vec{v}'_{\perp})}{dt} = m \frac{d\vec{v}'_{\perp}}{dt} = q(\vec{E}_{\perp} + \langle \vec{v}_{\perp} \rangle \times \vec{B} + \vec{v}'_{\perp} \times \vec{B}) = q\vec{v}'_{\perp} \times \vec{B}$$

where the value from (2.13) has been used to simplify the previous identity.

Hence, the perturbation corresponds to a circular motion around the guiding center. This same process can be followed in order to obtain drift equations for many other forces when they are combined with magnetic fields. This approach is the **drift-kinetic theory**.

Following the same procedure, the equation of motion can be also averaged to obtain the drift associated to joint action of the magnetic field and any further external force,  $\vec{F}$  (gravitational, centrifugal due to the bending of the magnetic fields...):

$$\vec{v}_F = \frac{\vec{F} \times \vec{B}}{qB^2} \quad (2.14)$$

If the force does not depend on the charge, this magnetic drift will be different for ions and electrons. This general procedure can be extended to introduce another drifts (whose derivation is in Appendix A.1):

$$\vec{v}_{\nabla B} = -\frac{m}{2B^2} \cdot \frac{v^2}{q} \left( \vec{B} \times \vec{\nabla} B \right) \quad \text{known as grad-B drift} \quad (2.15)$$

$$v_e = -\frac{\vec{\nabla} p \times \vec{B}}{qnB^2} \quad \text{diamagnetic drift} \quad (2.16)$$

### 2.2.2 The magnetic dipole moment

The motion of a charged particle within a magnetic field is composed by the motion of its guiding center (which can be studied using the drift-kinetic theory) plus a circular motion around it. This circular motion can be understood as a circular electric current, so it is possible to define a magnetic dipole moment:

$$\|\vec{\mu}\| = \frac{|q|\omega_c}{2\pi} \cdot 2R_c = \frac{E_{kin,\perp}}{B}$$

where  $\omega_c$  and  $R_c$  are the cyclotron frequency and radius (see figure 2.1), respectively. The last equality is derived from the fact that the total kinetic energy can be decomposed in a kinetic part depending on the velocity parallel to the magnetic field and its

perpendicular part, which is related to the dipole moment. An important property of this moment can be derived using the *adiabatic invariance theorem*:

$$J = \oint mv_x dx = \oint mv_x^2 dt = \int_0^{2\pi/\omega_c} mv_{\perp}^2 \sin^2(\omega_c t + \phi) dt = \frac{\pi m_{\perp}^2}{\omega_c} = \frac{2\pi m}{|q|} \mu$$

where *sin* appearing corresponds to a generic circular motion, whose frequency is the Larmor frequency.

If we consider a time-dependent magnetic field that varies slower enough than the gyro-period, then the action (J) and, consequently, the magnetic dipole moment are **adiabatic invariants**. If the variation of the external parameters, i.e., the magnetic field is slow enough, these quantities can be considered as constants of motion.

### 2.2.3 The need for a tokamak

Confinement of charged particles is only ensured in the perpendicular plane to the magnetic field lines due to the circular motion around them, but not in the parallel direction. The confinement in this parallel direction can be obtained by properly bending the magnetic field lines such that they are closed within a certain device, like a torus (as shown in figure 2.2).

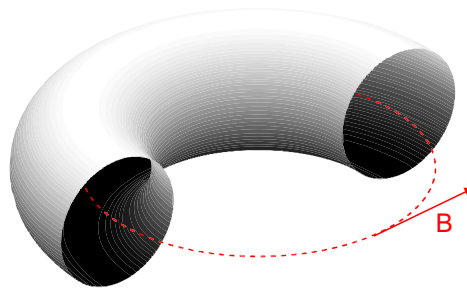


Fig. 2.2 Closed field lines system

In closed field lines systems, there are some important properties:

1. Since the coils are more concentrated on one side than on the other, the magnetic field in the inner part (**High-field side(HFS)**) is much stronger than in the

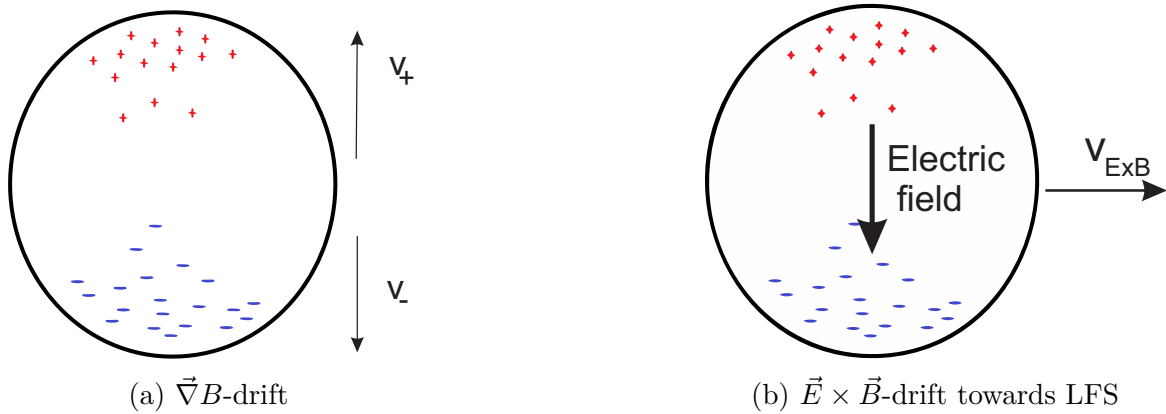


Fig. 2.3 Drifts in a purely toroidal-symmetric system.

outer part (**Low-field side(LFS)**). This leads to a gradient in the magnetic field intensity and, thus, to a drift effect, as shown in figures 2.3). This drift will produce a charge separation (in figure 2.3a, ions will move upwards, while electrons move downward).

2. This charge separation will produce an electric field between the upper and bottom parts, thus causing a  $\vec{E} \times \vec{B}$  drift towards the LFS (2.3b).

In these systems, particle confinement is not good enough, but the introduction of 3D magnetic configuration will eventually inhibit these drifts and the losses:

- **TOKAMAK CONCEPT:** here, the poloidal field is produced by an inductively driven plasma current leading to a toroidal geometry. This current is induced by a transformer which uses the plasma as a secondary coil.
- **STELLARATOR CONCEPT:** both magnetic field components are produced by helically wound external coils, thus leading to a 3D configuration.

In this work, the tokamak approach is presented. In general, modern tokamaks have not the shape of a circular torus, but a more elongated cross section such that they can be more compact. In figure 2.4 the general structure of a tokamak is presented, showing different parts:

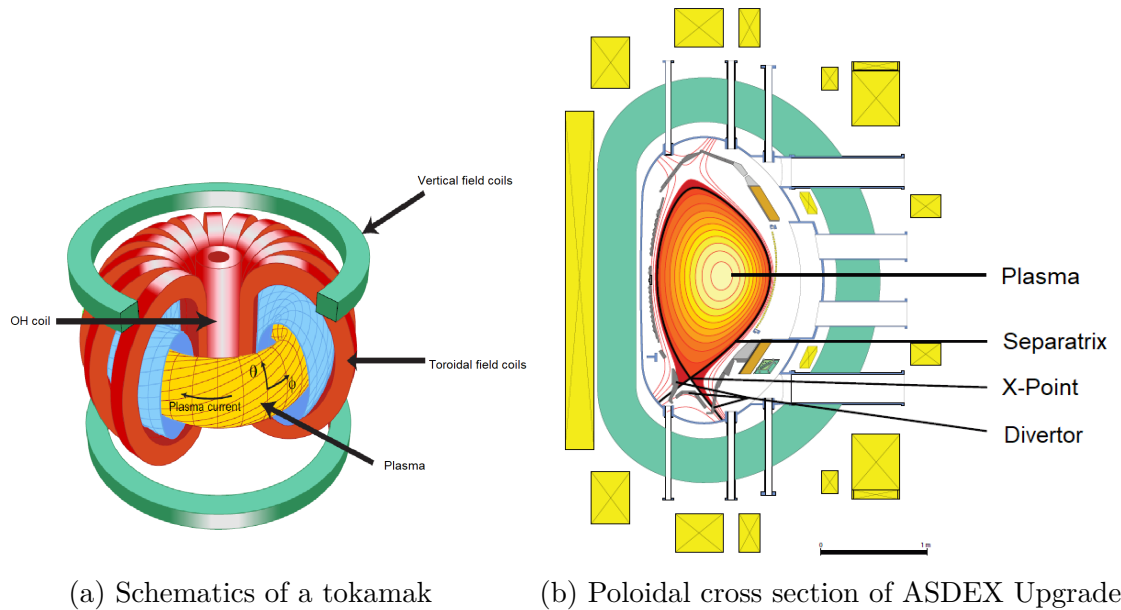


Fig. 2.4 Main physical features of a circular Tokamak [From IPP Database].

1. D-coils: due to the elongated cross-section of tokamak, D-shaped coils rather than circular coils are used.
2. Vertical coils: control vertical position of the plasma and are also used for plasma shaping.
3. OH coil: this coil is used as the primary coil in a transformer where the secondary coil is the plasma itself and heats it through ohmic heating. It is also used to induce the current in the plasma.

Another important part, not shown in that figure, is **Neutral Beam Injector, NBI** which injects a neutral particles with a high kinetic energy in order to heat the plasma. The mechanism to create this neutral injection is accelerating charged particles and then re-neutralizing them such that they do not suffer from magnetic forces until they reach the plasma and start heating it.

The induced current will create a poloidal magnetic field (which is conventionally less intense than the imposed toroidal field in tokamaks). The combination of both field components leads the magnetic field line to twist and follow helical-like paths.

These magnetic flux surfaces are either closed or opened (see figure 2.4b). The last closed flux surface (LCFS) is also known as **separatrix** and separates the confined plasma from open field lines. This separatrix also has a singular point: the **X-point**. The singularity consists on the crossing of two magnetic field lines (of the poloidal component) leading to a vanishing poloidal magnetic field in that point.

Another important parameter is the safety factor,  $q$ :

$$q = \frac{\Delta\phi}{2\pi} \approx \frac{rB_\varphi}{RB_\theta} \quad (2.17)$$

where  $\Delta\phi$  is the change of the toroidal angle when a magnetic field line travels a full poloidal loop and  $R$  is the major radius. The second expression is usually used for the safety factor.

Following the drift-kinetic theory, it becomes clear that the motion of single particles within the plasma depends on their velocity parallel to the magnetic field, due to a gradient in the magnetic field. If their parallel speed is not high enough there will be some point in which the magnetic field becomes so high that a magnetic mirror force appears which causes the particles to be reflected at the mirror positions (in blue in fig. 2.5): they are called **trapped particles** and their orbits are known as *banana orbits*. Other particles will be able to overcome this force (in black in fig. 2.5): these are called **passing particles** and their orbits, *potato orbits*.

## 2.3 Toroidal Alfvén Eigenmodes

Magnetohydrodynamics instabilities that are due to the non-linearity of the MHD equations can degrade the confinement. In the present work, instabilities that can be induced by the existence of fast-ions (supra-thermal particles, like fusion-born  $\alpha$  particles or particles injected by NBI) are studied. These are called *Toroidal Alfvén eigenmodes*, (*TAE*) [6, 7].

Within MHD framework, it is possible to study whether a certain perturbation from the equilibrium, is stable or not. The simplest analytical approach to study the

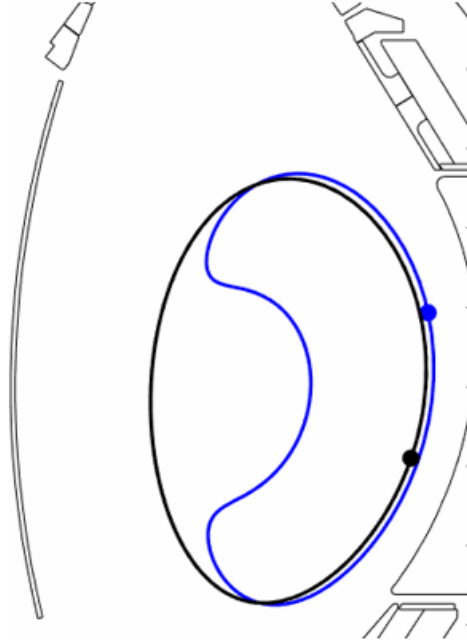


Fig. 2.5 Motion of particles within tokamaks. The **black** line represents passing particles and the **blue**, trapped particles. [J. Gonzalez-Martin]

stability is to linearize the equations (Derived in appendix A.1.) and then use the Fourier transform technique in the time coordinate. A compact way of writing the momentum equation is:

$$\rho \frac{\partial^2 \vec{\xi}}{\partial t^2} = \vec{F}(\vec{\xi})$$

where,  $\vec{F}(\xi)$  is the force operator (by analogy with Newtonian case) and  $\vec{\xi}$  represents a plasma displacement, with respect to the equilibrium situation. Using the convention of denoting by subindex 0 the equilibrium values and by subindex 1 the perturbation around the equilibrium, the force operator can be rewritten as:

$$\vec{F} \approx \vec{J}_1 \times \vec{B}_0 + \vec{J}_0 \times \vec{B}_1 - \vec{\nabla} p_1$$

By combining properly the linearized equations the force operator can be rewritten only in terms of the equilibrium values [6]:

$$\vec{F}(\vec{\xi}) = \vec{\nabla} \left[ \vec{\xi} \cdot \vec{\nabla} p_0 + \gamma p_0 \vec{\nabla} \cdot \vec{\xi} \right] + \frac{1}{\mu_0} \left\{ \vec{\nabla} \times \vec{\nabla} \times (\vec{\xi} \times \vec{B}_0) \times \vec{B}_0 + (\vec{\nabla} \times \vec{B}_0) \times (\vec{\nabla} \times (\vec{\xi} \times \vec{B}_0)) \right\} \quad (2.18)$$

In this linearized form it is possible to make a Fourier analysis in time so we can find an eigenvalue equation for the frequency [7]:

$$-\rho_0 \omega^2 \vec{\xi} = \vec{F}(\vec{\xi}) \quad (2.19)$$

Since the force operator is Hermitian,  $\omega^2$  can only be real so we will have either purely exponential growth (instabilities) or oscillatory behavior (stable). Moreover, it also implies that these modes are independent of each other. This is only valid as long as the perturbation is small enough. If the perturbation had a large amplitude the linear approach is not longer valid and the non-linear theory has to be used.

Previous results can be applied to the special case of the toroidal geometry (see figure 2.4a). In such geometries, special symmetries exists can be used to obtain further simplifications, using a Fourier expansion in the angular space:

$$\vec{\xi}(r, \theta, \phi) = \sum_{m,n} \vec{\xi}_{mn} e^{i(n\phi - m\theta - \omega t)} \quad (2.20)$$

where  $\phi$  is the toroidal angle (centered at Z-axis) and  $\theta$  is the poloidal angle, measured from the circle in which the torus is centered.

Under the assumption of a purely toroidal symmetry, the decomposition components are independent. Nonetheless, in real tokamaks this symmetry is broken:

- In the poloidal direction ( $\theta$ ), the value of the magnetic field changes along the radial value, thus inducing a dependence  $\vec{B} = \vec{B}(\theta)$ .
- in the toroidal direction ( $\phi$ ), the continuous symmetry is broken due to the finite number of coils: between two consecutive coils there appears a certain toroidal

field ripple that induces this breakup. As an approximation, this ripple in the magnetic field is negligible and the toroidal symmetry is not broken.

Under these assumptions, the toroidal components can be still considered as independent, but the asymmetry in  $\theta$  leads to a coupling in the poloidal components. Despite of that, equation (2.19) can be still considered, with the appropriate form of the force operator when the Fourier decomposition is used. According to the previous approximation it is useful to consider the toroidal modes as independent, so the eigenvalue equation can be studied for all the  $n$ -modes independently. On the other hand, the poloidal modes ( $m$ -modes) will not be independent and will interact among them. A good approximation for this mode entangling is to allow for the closest poloidal modes to interact, i.e., it should be considered that the  $m$ -mode is coupled only to  $m\pm 1$ -modes.

Using the approach of ref. [6], the eigenvalue equation (for radial perturbations) can be written as [8, 9]:

$$\frac{d}{dr} \left[ (\rho\omega^2 - F^2) r^3 \frac{d\xi_{nm}}{dr} \right] - (m^2 - 1) (\rho\omega^2 - F^2) r \xi_{nm} + \omega^2 r^2 \frac{d\rho}{dr} \xi_{nm} = 0$$

where we have already disregarded the subscript 0 and  $r$  corresponds to the radial distance (of the cylindrical coordinates). The function  $F = F(r)$  is defined as:

$$F \equiv (m - nq(r)) \frac{B_\theta}{\mu_0^{1/2} r}$$

From the eigenvalues equation a singularity in the highest derivative order appears:

$$m - nq(r) = \pm \frac{\omega r}{B_\theta / (\mu_0 \rho)^{1/2}}$$

leading to continuum spectra of frequencies for each mode ( $n, m$ ). It can be quickly seen, in  $\omega^2 - q(r)$  diagram (fig. 2.6), that  $m$ -modes has crosses among them. Due to these crosses in  $\omega^2 - q(r)$  diagram, in points close to such crossing the solution obtained for  $\omega(r)$  is not longer valid and the  $m$ -modes will couple. These modes will break and

rejoin in the neighborhood of such points, leaving a gap. In these gaps discrete modes known as **Toroidal Alfvén Eigenmodes** (TAE) appear.

There is an important feature of this TAE that differentiates it from the continuum spectra. TAEs suffer from less damping than the continuum frequencies, and thus it is possible to overcome such a damping. In particular, fast-ions could interact with this mode and destabilize it. This kind of instability has been experimentally observed in many tokamaks experiments [8, 9].

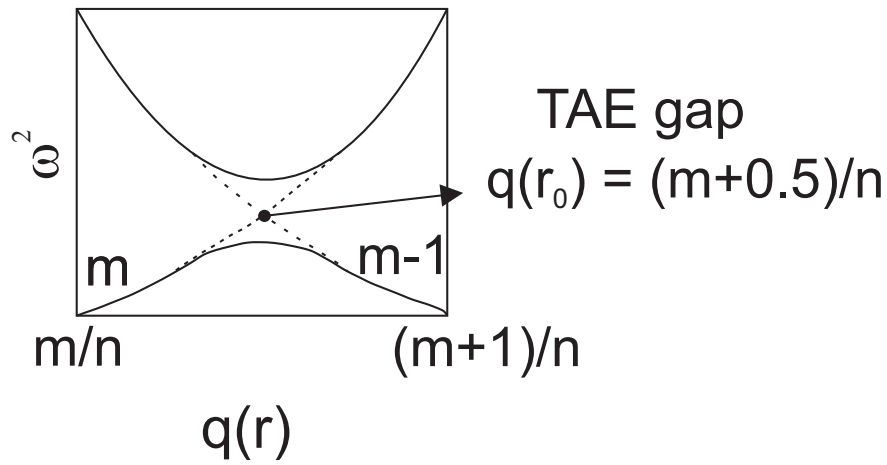


Fig. 2.6 Appearing of the gap mode [7].

The relation between the safety factor and the mode numbers is:

$$q(r) = \frac{m + 1/2}{n} \quad (2.21)$$

this also enables the determination of the radial location of TAEs, i.e., on which flux surface the TAE is excited.

A more deep analysis would require taking into account that  $m$ -modes are coupled (within the same  $n$ -mode), which can be done by coupling the mode equation [7].

# Chapter 3

## The physical framework: MEGA

In chapter 2, the plasma has been modelled as a fluid, which implies the coupling of the Navier-Stokes with the Maxwell equations. The most general description, equations (2.2)-(2.5), is a non-linear partial differential equation (PDE) system that couples all the terms in the equation making the analytical solution impossible. In addition, fast-ions and their interaction with the bulk plasma need to be taken into account. This separation between bulk plasma and fast-ions comes from the gap between their energies between both. The bulk plasma has energies of about 10 keV while fast-ions have much larger energies (e.g., fusion-born  $\alpha$  particles have energies of 3.5 MeV or injected neutral, about 90 keV), making their dynamics to be very different. Due to these issues, numerical procedures are the only available approach to have more realistic results, instead of using simplification techniques like linearization. The advantage of the numerical procedures, apart from solving a more realistic problem, is that it also allows for more complex geometries to be implemented, like the ASDEX Upgrade (AUG) tokamak (as shown in 2.4b).

This chapter is dedicated to MEGA [10, 11], a numerical 3D nonlinear hybrid kinetic MHD model dedicated to compute the solution of such complex equations. In the following sections both the physical and mathematical background are briefly discussed and finally, the problem of the boundary conditions is stated.

### 3.1 The physical background: Hazeltine-Meiss model

The plasma is divided in two interacting parts, the bulk plasma and the fast-ions, where the current and pressure of fast-ions must be taken into account in the MHD equations. A joint set of equations that properly couple both bulk plasma and fast-ions is needed. In MEGA, a new term in the the momentum equation is introduced to take into account the current density of the fast-ions.

In MEGA, a more realistic model than resistive MHD is needed, called the extended Hazeltine-Meiss MHD model (HM) [12]. In this model, dissipative effects have been introduced through viscosity and diffusivity parameters along with effects like plasma rotation and the influence of the fast-ions [11, 13]:

$$\begin{aligned}
\frac{\partial \rho}{\partial t} &= -\vec{\nabla} \cdot (\rho \vec{v}_b) + \nu_n \vec{\nabla}^2 (\rho - \rho_{eq}) \\
\vec{\omega} &= \vec{\nabla} \times \vec{v} \quad \text{Fluid vorticity} \\
\rho \frac{\partial \vec{v}}{\partial t} &= -\rho \vec{v}_b \cdot \vec{\nabla} \vec{v} + \rho \vec{v}_{pi} \cdot \vec{\nabla} (v_{\parallel} \vec{b}) - \vec{\nabla} p + (\vec{J} - \vec{J}'_{\alpha}) \times \vec{B} + \frac{4}{3} \vec{\nabla} (\nu \rho \vec{\nabla} \cdot \vec{v}) - \vec{\nabla} \times (\nu \rho \vec{\omega}) \\
\frac{\partial p}{\partial t} &= \vec{\nabla} \cdot (\rho (\vec{v} + \vec{v}_{tor})) - (\gamma - 1) p \vec{\nabla} \cdot (\vec{v} + \vec{v}_{tor}) + (\gamma - 1) [\nu \rho \|\omega\|^2 + \frac{4}{3} \nu \rho (\vec{\nabla} \cdot \vec{v})^2 \\
&\quad + \eta \vec{J} \cdot (\vec{J} - \vec{J}_{eq})] + \chi \vec{\nabla}^2 (p - p_{eq}) \\
\frac{\partial \vec{B}}{\partial t} &= -\vec{\nabla} \times \vec{E} \\
\vec{J} &= \frac{1}{\mu_0} \vec{\nabla} \times \vec{B} \\
\vec{E} &= -\vec{v}_E \times \vec{B} - \vec{v}_{tor} \times (\vec{B} - \vec{B}_{eq}) + \eta (\vec{J} - \vec{J}_{eq})
\end{aligned}$$

In this equation, the total velocity of the bulk plasma is divided in three terms:

$$\vec{v}_b = \vec{v} + \vec{v}_{tor} + \vec{v}_{pi}$$

where the velocity without subindex is the velocity described by the MHD equations, that is corrected with two additional terms, the toroidal velocity and the diamagnetic drift. Due to the NBI configuration and also transport phenomena, the injected

fast-ions induce an extrinsic angular momentum, producing the spin of the plasma around itself. The diamagnetic drift is a correction, to this one-fluid model, that takes into account the difference between the electrons and ions present in the plasma. Both electrons and ions carries a certain dipole moment, resulting that the plasma is naturally diamagnetic.

A force can be associated to the pressure gradients, such that a drift can be found by following expression (2.14):

$$\vec{v}_{prs} = \frac{\vec{B} \times \vec{\nabla} p}{qnB^2}$$

where  $q$  is the electron elementary charge (in absolute value) and  $n$  is the electron density.

Dissipative effects in plasma are taken into account by including the resistivity ( $\eta$ ), viscosity ( $\nu$ ), compressibility ( $\nu_n$ ) and the diffusivity ( $\chi$ ). Finally, the momentum equation contains a term in which the fast-ions current,  $\vec{J}'_\alpha$ , appears explicitly. All these equations are coupled nonlinear PDE equations (with initial and boundary conditions are discussed in sections 3.2 and 3.4, respectively). Due to the symmetries present in tokamaks, MEGA implements a regular grid in cylindrical coordinates and fourth-order finite differences scheme, i.e., each partial derivative is approximated using a Taylor expansion up to the fourth order. A fourth-order Runge-Kutta method is applied for the time integration, as well.

For the motion of the fast-ions, drift-kinetic theory becomes useful, allowing the reduction of the dimensionality of the problem. Here, only the guiding-center motion is studied, removing one component in the velocity-space. Still, the gyro-motion can have an important effect on the stabilization of certain instabilities, so in the simulations, there are also corrections to take into account the finite Larmor radius (FLR) as seen in figure 3.1. Here the PIC formalism is used: instead of evolving each particle, which requires a large numerical effort, a set of markers is considered. Markers represents a set of these fast-ions with total charge and mass that represents all the particles, eventually reducing the computational issue. This marker approach is based on the

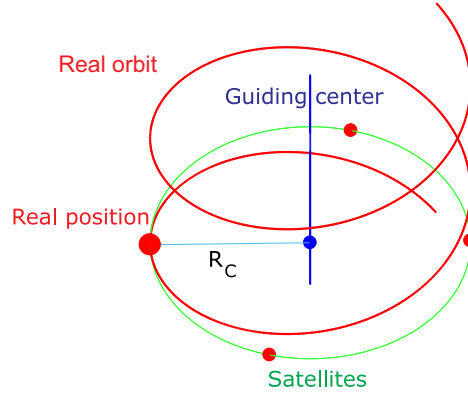


Fig. 3.1 Geometrical representation of satellites approach. The time evolution is considered for the guiding center (blue), but a more realistic evolution requires to take into account FLR effects. Instead of studying the electromagnetic fields of guiding center, the ones created by virtual particles located in a circumference with Larmor radius  $R_c$  around it (circumference in red), i.e., the projection of the helix motion onto the plane (in green). Consequently, the gyro-phase is neglected and this method is only an approximation of the actual motion (helix, in red).

Boltzmann equation (2.1): for each marker a partial distribution function,  $f_\alpha$ , can be associated, such that each one fulfills equation (2.1) [6].

The guiding-center dynamics can be described as:

$$m_\alpha v_{\parallel} \frac{dv_{\parallel}}{dt} = v_{\parallel}^* (q_\alpha \vec{E} - \mu \vec{\nabla} B) \quad (3.1)$$

where  $v_{\parallel}$  is the velocity parallel to magnetic field line and  $v_{\parallel}^*$  is the parallel velocity with a FLR correction:

$$v_{\parallel}^* = v_{\parallel} [\vec{b} + R_c \vec{\nabla} \times \vec{b}]$$

The dynamics of fast-ions is, therefore, described as charged particles (with charge  $q_\alpha$ ) and a magnetic dipole moment,  $\mu$ . The FLR correction to the parallel component (parallel to magnetic field) can be understood a magnetic field unit vector ( $\vec{b}$ ) and a Taylor expansion around the helix motion.

The total velocity of the particle consists on this corrected parallel velocity and all the drifts discussed. Similarly to the HM equations, the numerical integration of the equation for fast-ions is done through a fourth-order Runge-Kutta scheme.

## 3.2 Initial conditions: equilibrium and initial profiles

In the previous section, the HM model has been introduced, but the particular solutions require from the proper boundary and initial conditions. The solutions of the MHD equations provide the time evolution of the magnetic fields and the pressure, among others. In order to solve the MHD equations, an initial magnetic field configuration and profiles for temperature and density for electrons are needed. In this one-fluid MHD model, the electron density and temperature are only considered

In MEGA, the initial magnetic field configuration is taken from an equilibrium situation, described by the ideal-MHD model (2.7) - (2.12). In the equilibrium, there is a relation between the scalar pressure and magnetic field configurations, known as *force balance equation*:

$$\vec{J} \times \vec{B} = \vec{\nabla} p \quad (3.2)$$

which can be derived from ideal MHD equations by considering the steady state ( $\partial/\partial t \rightarrow 0$ ).

There is a more convenient formulation of the force balance equation using flux coordinates instead of cylindrical coordinates [7, 14] (see figure 3.2). This system is based on three coordinates related to the magnetic field:  $\psi$  is the poloidal magnetic flux and  $\theta$  and  $\varphi$  are the poloidal and toroidal angles.

Defining the following two functions:

$$\begin{aligned} \vec{B} &\equiv \frac{1}{R}(\vec{\nabla}\psi \times \vec{u}_\phi) \\ f(\psi) &= \frac{R}{B_\phi}\mu_0 \end{aligned}$$

it is possible to rewrite (3.2) as an elliptic equation that can be solved numerically, the **Grad-Shafranov equation** [6, 14], whose derivation is shown in Appendix A.3:

$$R \frac{\partial}{\partial R} \left( \frac{1}{R} \frac{\partial \psi}{\partial R} \right) + \frac{\partial^2 \psi}{\partial z^2} = -\mu_0 R^2 p'(\psi) - \mu_0^2 f(\psi) f'(\psi) \quad (3.3)$$

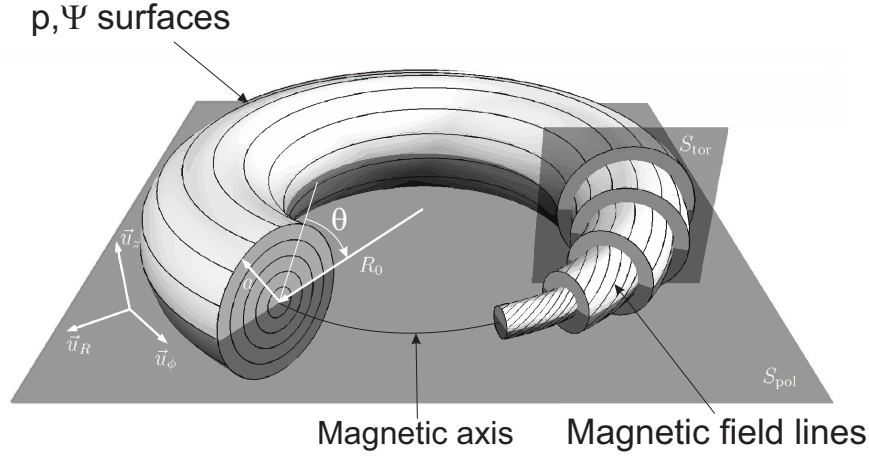


Fig. 3.2 Magnetic coordinates [15]. Poloidal and toroidal fluxes,  $\Psi$  and  $\Psi_{tor}$ , are the magnetic fluxes that go across of circular surfaces,  $S_{pol}$  and  $S_{tor}$ , centered in Z-axis and in the circumference with radius  $R_0$ , respectively.

This equation can be solved for some initial conditions. In particular, this initial profile consists on the experimental values of pressure in AUG experiment, resulting in magnetic equilibrium as shown in 3.4, which will be used in MEGA as starting distributions.

The initial conditions of densities and temperatures are used in MEGA in order to characterize the pressure. This initial conditions are also taken combining the experimental measurements from different diagnostics, as seen in 3.3.

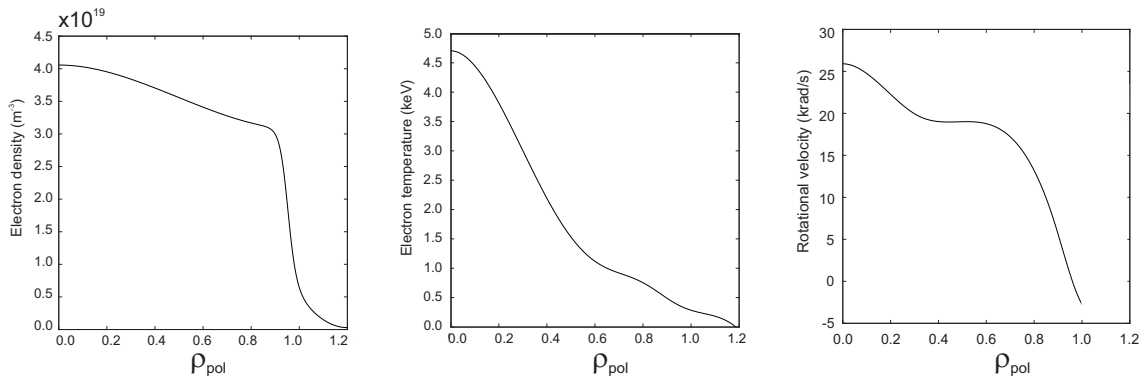


Fig. 3.3 Input profiles in MEGA obtained from IPP, with the corresponding experimental measurement [16] corresponding to the discharge #34570 from AUG in the time window 3.300-3.400 ms. A new radial coordinate is defined  $\rho_{pol} = \sqrt{\frac{\psi - \psi_0}{\psi_{LCFS} - \psi_0}}$ , where  $\psi_0$  is the magnetic flux at the magnetic axis,  $\psi_{LCFS}$  is the flux at the separatrix.

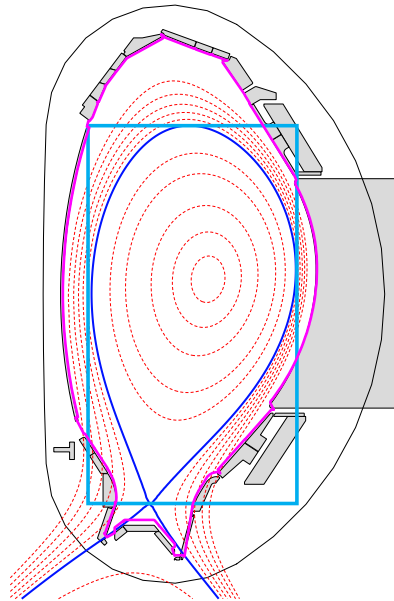


Fig. 3.4 Magnetic equilibrium for discharge #34570. The flux surfaces are shown in red dashed lines, whereas the separatrix is shown in blue. The blue rectangle is the simulation domain and actual 2D wall is shown in magenta. From this figure, it is clear that the simulation domain is containing parts that are outside the vessel.

### 3.3 Fast-ions

Fast-ions are particles with energies that are larger than those typical of thermalized plasmas (about 10 keV). The study of these particles and how they interact with the bulk plasma, i.e., the thermalized plasma, has a central importance in the fusion research. Fast-ions, either fusion-born  $\alpha$  particles or high-energy neutral particles injected with NBI, plays a fundamental role in the plasma heating and energy production, since these fast-ions must provide the energy the plasma needs to sustain the fusion reactions for long times. The fast-ion confinement is, nowadays, an important research line.

Fast-ions in the plasma are described using a statistical approach by giving a certain distribution function. The equilibrium distribution function can be derived from a Fokker-Planck equation<sup>1</sup>, leading to the **slowing down distribution** [13]:

<sup>1</sup>Subject outside of the scope of this work.

$$f(\Psi, v, \lambda) = C e^{-\frac{\Psi}{\Psi_{scale}}} \frac{1}{v^3 - v_{crit}^3} \operatorname{erfc} \left( \frac{v - v_{birth}}{\Delta v} \right) e^{-\frac{(\lambda - \lambda_0)^2}{(\Delta \lambda)^2}} \quad (3.4)$$

where  $C$  is a constant that properly normalize the distribution function to the total energy of the fast-ions.

1. The first exponential describes the spatial distribution:  $\Psi$  is the toroidal magnetic flux coordinate, as discussed in previous section, and  $\Psi_{scale}$  is a parameter characterizing the gradient of fast-ions. In the simulations, it has been taken  $\Psi_{scale} = 0.15$ , but other values can be studied.
2. The next two factors characterize the velocities distribution (in modulus),  $v$ . Three parameters are here introduced:  $v_{crit}$ , which is the critical velocity at which collisional friction of fast-ions with both electrons and ions is equal. The critical velocity is a function of the magnetic field configuration, so it depends on the equilibrium choice.  $v_{birth}$  is the neutral beam injection velocity and  $\Delta v$ , small velocity (compared to  $v_{birth}$ ), is used to set the cutoff width. The cutoff velocity is usually set to 10% of the birth velocity.
3. Last term is referred to the pitch angle distribution. Pitch angle,  $\lambda$ , is the fraction of the velocity parallel to the magnetic field. In this work, the convention taken for pitch angle is assigning a negative sign:

$$\lambda = -\frac{v_{\parallel}}{v}$$

where  $v_{\parallel}$  is the parallel velocity (using the already discussed magnetic field convection) and the sign is given by the fact that in AUG magnetic field and electric current have opposite signs. This new term allows the separation of fast-ions in two type: co-going particles, that have negative pitch angle (in this convention), and counter-going particles. Besides the pair energy and pitch angle,  $(E, \lambda)$  can fully describe the velocity space of fast-ions within the MEGA model, since the third component of such velocity space would be the gyro-phase,

which is neglected in MEGA. The distribution in pitch angle follows a Gaussian distribution centered at  $\lambda_0$  with a width  $\Delta\lambda$ .

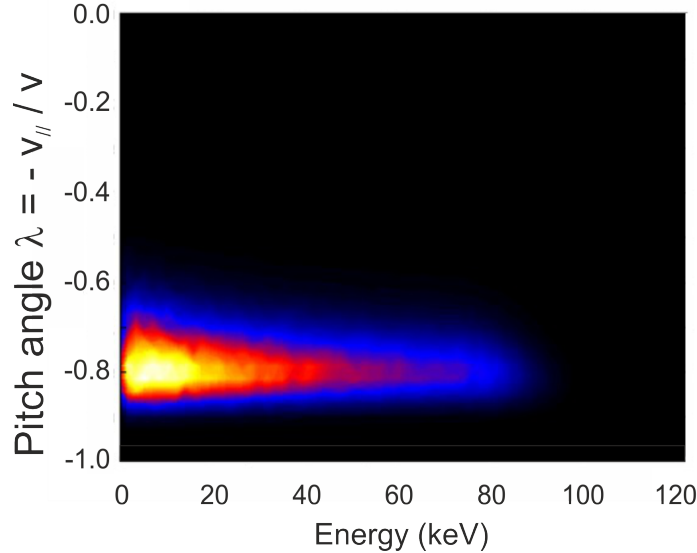


Fig. 3.5 Velocity space of the slowing down distribution, centered at  $\lambda_0 = -0.8$  with a width  $\Delta\lambda = 0.1$ . This configuration corresponds to the one the Neutral Beam Injectors (NBI 8) in the ASDEX Upgrade tokamak. The birth velocity of the beam is set to  $v_{birth} = 2.98 \cdot 10^6 \text{ms}^{-1}$ . Only co-going ( $\lambda < 0$ ) fast-ion distribution are relevant in this initial distribution function, and only negative pitch angles are here shown.

### 3.4 The simulation domain and the boundary conditions

Here, the need of studying which would be the appropriate simulation domain is presented. Most of the plasma is assumed to be confined within the separatrix, so the simulation domain must necessarily contains the whole separatrix volume (see figure 3.4).

Since the numerical integration uses a regular grids for integration, regions outside from both separatrix and the vessel are being considered for the evolution of either MHD plasma and fast-ions. Although plasma is mainly confined within separatrix,

the boundary conditions imposed, up to now, are not realistic. A realistic wall can affect the plasma and its stability [6], so its study becomes important. The boundary conditions considered previous to this work were:

- All the components of the speed vanishes at the boundaries (blue color in figure 3.4).
- The magnetic field at these boundaries remains unperturbed from its initial value. This approach makes sense when considering that are well apart from the separatrix, but it is clear that there are points in which the simulation domain is close to the separatrix, so this boundary conditions are not realistic at all.

These boundary conditions, despite of giving good results [17] are still unrealistic, so more realistic boundary conditions are required, trying to fit the wall.

This same issue appears for markers: markers are only considered as losses only if they scape from simulation domain. The implementation of the a realistic wall for fast-ions has important consequences, allowing to study the impact of losses along a realist wall and synthetic Fast-Ion Loss Detector (FIELD) whose data can be compared to experimental data.

# Chapter 4

## The MEGA wall: towards a synthetic FILD in MEGA

In this chapter the implementation of the wall in MEGA is discussed. A numerical background of the simulation code is briefly presented, continuing with the approach followed in this work to implement such wall and the advantages that it implies. Finally, the results from the performed simulations are presented.

### 4.1 Numerical background

To have a good accuracy in the time integration, a time step small compared to the gyro-period (related to the gyro-period) must be chosen to avoid numerical instabilities [18]. This small time step (chosen to be 4% of the Larmor frequency) imposes a strong performance requirement.

Regarding the spatial integration, a fine mesh is required for numerical stability. As the evolution of the whole plasma is needed, a large domain must be considered (see figure 4.1), so the mesh must have several subdivisions to reach a minimum spatial accuracy. This involves also a considerable drawback because the solver must invert large matrices, slowing down the simulation.

All these issues combined with the small time step chosen leads to the use of more advanced numerical and programming techniques than the usual methods. These techniques include algorithms that work with many processors at the same time solving different parts of the spatial mesh, known as *parallelization*. In MEGA, this is done dividing the whole integration domain into *cores*, i.e., CPUs that solves part of the whole mesh (see figure 4.1). The communication among these cores is precisely the parallelization technique, and the library Open-MP [19] is applied to that goal. Moreover, each core also integrates all the markers of fast-ions that lie within the domain of the core.

The final results for all the numerical processes are several files containing the time evolution of all the relevant properties of the plasma such as density, and temperature, and its dynamical properties, like velocity and magnetic field that undergo a discrete Fourier transform (DFT) following the scheme proposed in equation (2.20), so the analysis of the toroidal and poloidal modes can be done.

## 4.2 A realistic 3D wall for MEGA: towards a synthetic FILD

The inclusion of a realistic wall shape in the simulation has a significant importance:

- Improvement in simulation times: only when the particles come out of the domain, they are stopped from evolving. With the wall, the markers are detected when they reach to the wall and are then conveniently stopped.
- From such an identification algorithm, important information can be obtained. In particular, if the accuracy of the numerical wall is high enough, the study of fast-ion losses becomes feasible. The reconstruction of the phase-space of the losses allows a comparison against experimental data from the Fast-Ion Loss Detector (FILD).

The methodology followed in this work is based on the pre-existing separation of the spatial domain into cores, and the mesh used to solve MHD equations. An important distinction is made: the term **mesh** is reserved to the limits of the spatial domain that is processed by each CPU (as shown in figure 4.1) and **sub-mesh** for the part of the MHD grid contained in each CPU.

### PIXELATION OF THE WALL

Taking into account all these considerations, the most straightforward procedure to implement the wall is to use the cores distribution and the MHD mesh as basis. The wall can be introduced by applying the *pixelation*, i.e., the whole domain is divided in a certain mesh (not to be confused with the cores or the sub-mesh) such that each volume element can be characterized by a flag, stating if this part of the mesh contains the wall, or not. *A priori*, the mesh used to *pixelate* the wall can be arbitrarily chosen, but using the already existing cores distribution has a natural advantage due to the parallelization in MEGA, since each CPU will handle its own markers. The very first approach is considering a distribution of cores that are outside, inside or contains part of the wall, such that all the particles reaching the cores containing part of the wall, will be stopped and then stored for post-processing. Moreover, the cores that have been detected to be outside are stopped from evolving their markers. This method was implemented and it has no impact on the computational performance, i.e., it does not slow down the simulation.

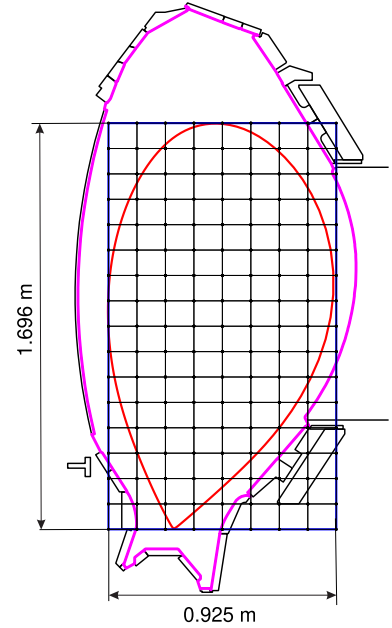


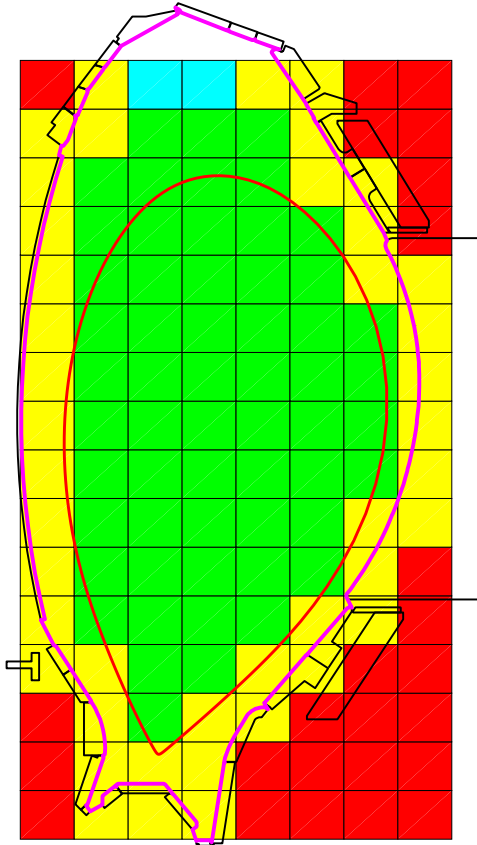
Fig. 4.1 Integration domain discretized (only the poloidal plane is represented, the subdivision in the toroidal angle is analogous). Each part of the domain will be partially integrated by one CPU and then all the data is communicated among all the CPUs to recompose the complete solution. The simulation can also be extended to cover a larger area of the tokamak.

Related to the time consumption, the pixelation of the wall can be done as part of a certain pre-process and then loaded into MEGA as a matrix, which allows the simulation only to check in which *pixel* the particle is (a simple integer quotient). The process of pixelation is done based on the Jordan curve theorem [20]: tracing rays starting from arbitrary points, whose relative position with respect to the wall is previously known, for instance, the Z axis of the tokamak, ending in test points, the parity of number of collisions with the wall will reveal if the point lies inside (odd number of crossings) or outside the wall (even number). Following that procedure recursively for all the points describing each pixel gives a map like the one shown in figure 4.2.

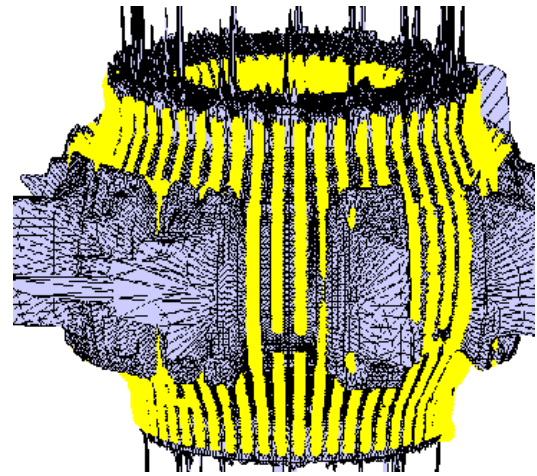
### 4.3 Simulations and discussion

Several simulations testing both accuracy and performance have been carried out. Among all these simulations, the evolution of discharge #34570 has been studied using the initial conditions shown in figure 3.3 along with its corresponding equilibrium. A thirty-hour simulation has been carried out reaching 0.18 ms of the plasma evolution from the initial equilibrium. A ( $R = 128, \phi = 32, Z = 256$ ) cylindrical grid has been chosen for the simulations. The initial conditions for MHD equations are also shown in figure 3.3, the initial distribution of fast-ions is a slowing-down distribution centered at pitch-angle  $\lambda_0 = 0.8$ , shown in figure 3.5.

In figure 4.3 the time evolution of the more interesting energies are presented. In the figure above, the time evolution of each toroidal mode is presented. The predominant modes are  $n = 5$  and  $n = 4$ , and its growth (in logarithmic scale) has three phases, an initial one in which the system is still close to the original equilibrium, a second phase, representing a linear growth and a final saturation. The non-linearity of the system of equations is also shown: when a mode starts growing it can interact with the other modes. In this case the first excited modes,  $n = 4, 5$ , interact with the lower  $n$ -modes, inducing, first, its linear growth and the later saturation. In the figure below,



(a) Overview of the grid showing the spatial distribution for cores. Sub-mesh distribution is analogous, showing a much better accuracy.



(b) Overview of the 3D grid and the ASDEX Upgrade mesh.

Fig. 4.2 Maps obtained from the pixelation of the 2D and 3D wall. On the left-hand side, the distribution using the core grid is shown. Each core can decide if it must study the position of each marker: if the core is completely inside (**green**), it evolves its markers without any further check, but if it contains part of the wall (**yellow**) then it check in which part of its sub-mesh the particle is, whose pixelation is analogous to the one shown, but with larger accuracy. Cores in **red** are not evolving realistic markers, so all of them are stopped from evolution. Finally, **blue**-cores are those in one of the limits of the simulation domain that do not contains any part of the wall, and it has to be studied whether the markers have escaped from the simulation domain. In right-hand side, the 3D wall pixelation is shown (only yellow sub-mesh points) compared to the real AUG wall, showing a good fit to the wall.

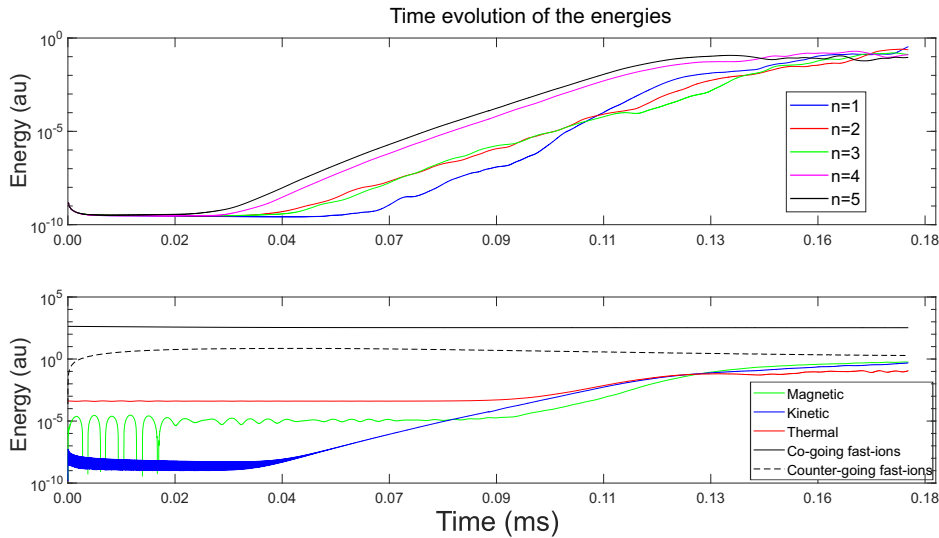


Fig. 4.3 Time evolution of different energies.

the evolution of the different kind of energies are shown: kinetic, magnetic and thermal, related to the bulk plasma energy and the black ones represents the total energy of the co-going fast-ions ( $\lambda < 0$ ). Counter-going particles ( $\lambda > 0$ ) are also drawn in dashed lines (positive pitch angle). It can be observed in the figure 4.3 below is that the kinetic energy of the fast-ions start to increase its energy from an approximate time of  $t \approx 0.05$  ms, which is approximately the time the first banana orbits (as it can be seen in figure 2.5) has reached their turning point.

A realistic 3D wall of ASDEX Upgrade has been implemented in MEGA code, enhancing considerably the study of role of the fast-ions during instabilities and the distribution of losses in the spatial space and in the velocity space.

In figure 4.4, the distribution of lost fast-ions during the simulation is presented, in a reduced version of the total velocity space (since the gyro-phase is neglected in the drift-kinetic approach), taking as parameters for representation energy and pitch angle of the losses. The figure shows the existence of three main lobes of losses: two main co-going losses lobes and a smaller lobe of counter-going particles. The main co-going losses lobe shows a shape similar to the initial slowing down distribution

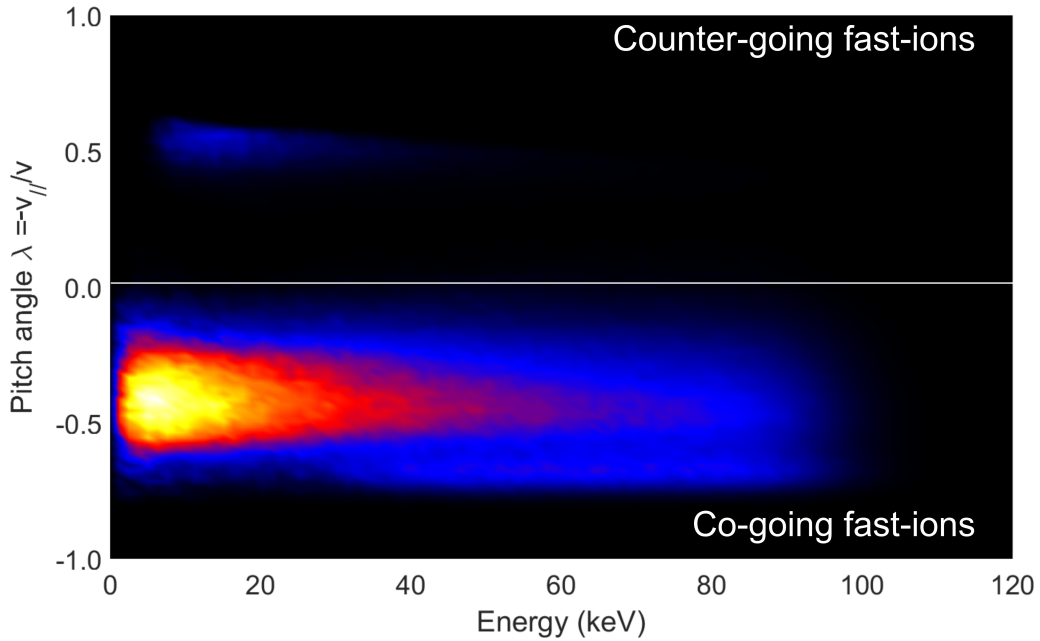


Fig. 4.4 (Reduced) Velocity space of the losses during the simulation.

function (shown in figure 3.5), but with a certain shift (due to the dependence of the pitch angle with the local magnetic field) and a larger dispersion, due to the scattering of the fast-ions. The counter-going fast-ion losses lobe is clearly the most remarkable feature we can observe since all particles are started as co-going particles, so they must have suffered from different processes to significantly change its value. A further study of this region of the velocity space lead to the fact that the losses producing that lobe are being lost against the divertor (DIV), as shown in figure 4.5.

### DIVERTOR REGION

In this section the simulated losses in the DIV region are presented.

In the set of figure 4.6 the spatial and velocity spaces distributions of the losses in DIV region are shown. In the velocity space two main lobes appears. The largest one corresponds to co-going particle losses with the initial pitch angle. For the smaller lobe, the counter-going particles losses lobe, time evolution of the accumulated particles



Fig. 4.5 Spatial distribution of the co-going lobe losses in 4.4.

arriving has been represented in figures 4.6c and 4.6d. A change in the behavior of the losses rate at  $t \approx 0.05$  ms can be observed, corresponding to the time in figure 4.3 where kinetic energy starts increasing, and the energy of the modes are growing as well. This can be understood as a first hint towards establishing that these particles are in fact being expelled because of the interaction with such modes. In this second time window (0.05 ms toward the end), the velocity space is represented in figure 4.7, showing that fast-ions with larger energies are mainly lost during the first time interval (from the start until 0.05 ms) showing that the registered high-energy losses are mainly prompt-losses: particles that have been lost during their first bouncing-back in their banana-like motion.

To study the existence of instabilities, the time evolution of the frequencies for each mode has been represented in 4.8. Only modes  $n = 4, 5$  show a well-defined frequency, that may correspond to TAE excitations [17, 21], according to figure 2.6.

These n-modes shows an stable frequency from, precisely, 0.05 ms time at which kinetic energy of the bulk plasma (bottom in the figure 4.3) starts linearly increasing, as

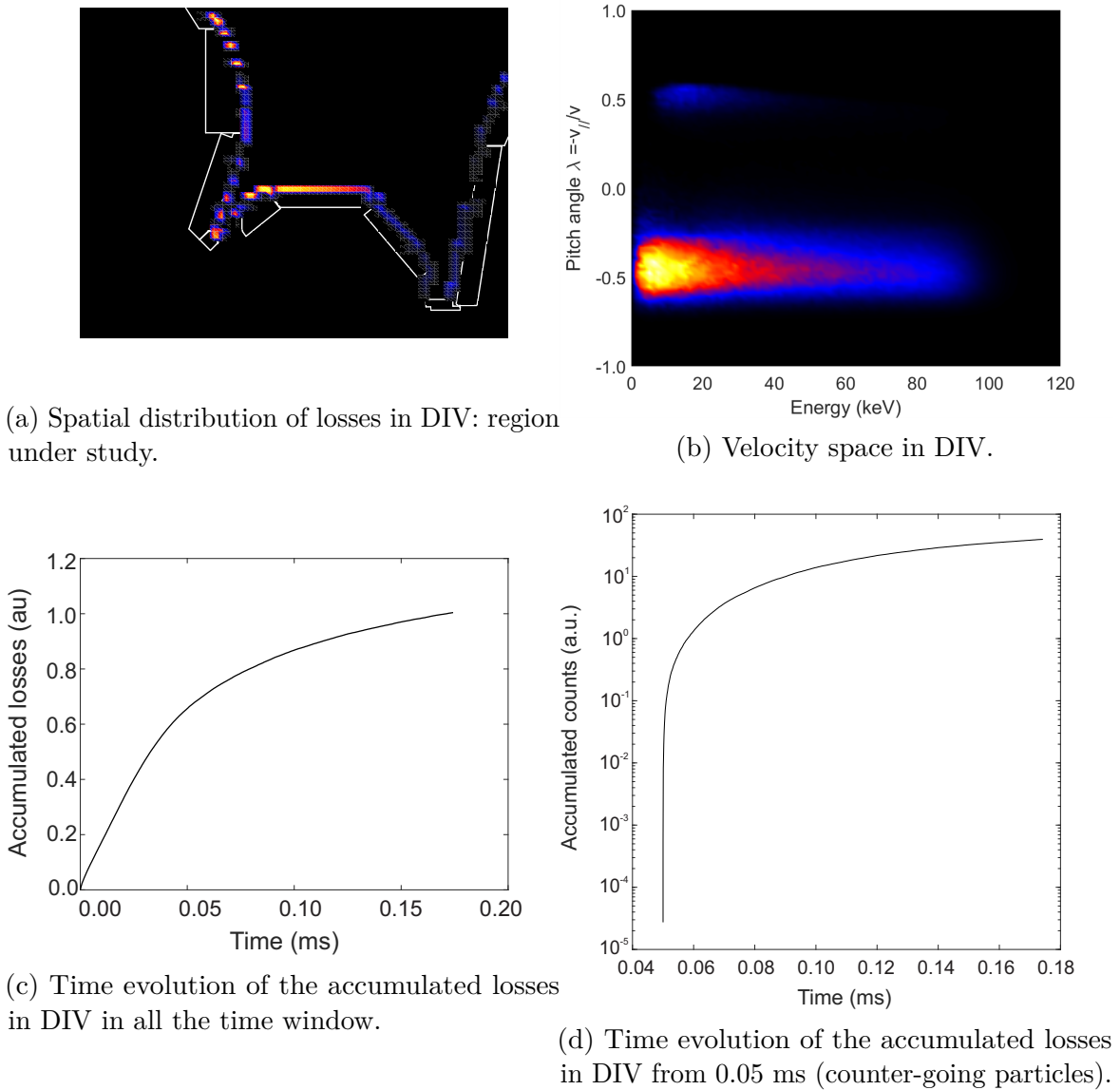


Fig. 4.6 Analyze of DIV losses. In figure (a) the spatial location of the losses, that are going to be studied, is shown. This spatial location is known as the divertor (DIV). In figure (b), the velocity space of the chosen spatial region is represented, showing two main lobes (a main co-going lobe and a smaller counter-going lobe). In figure(c), the losses accumulated in the DIV region is represented, showing two main dependences on time. Finally, in (d) the counter-going lobe is studied, showing that these particles are being lost from 0.05 ms.

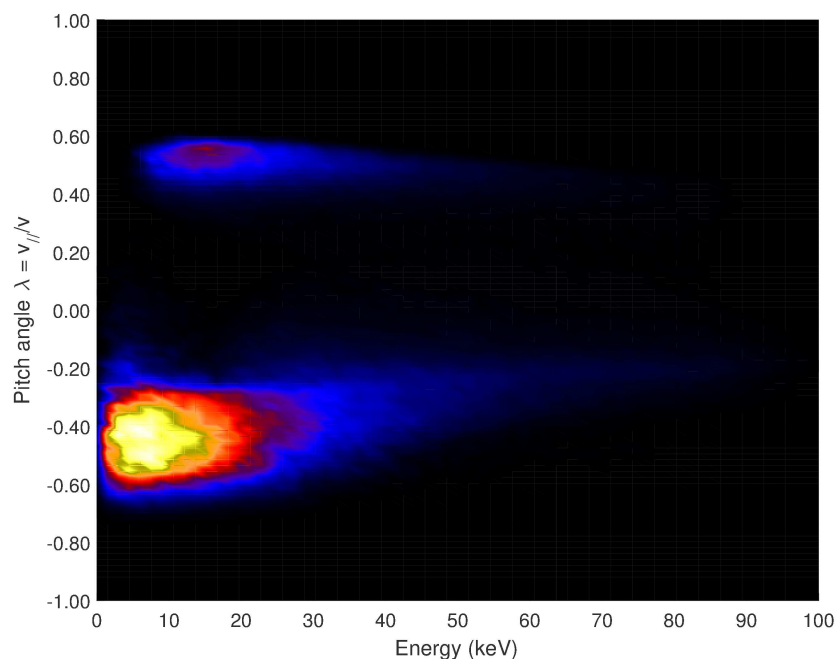


Fig. 4.7 Velocity space of losses in DIV from 0.05ms.

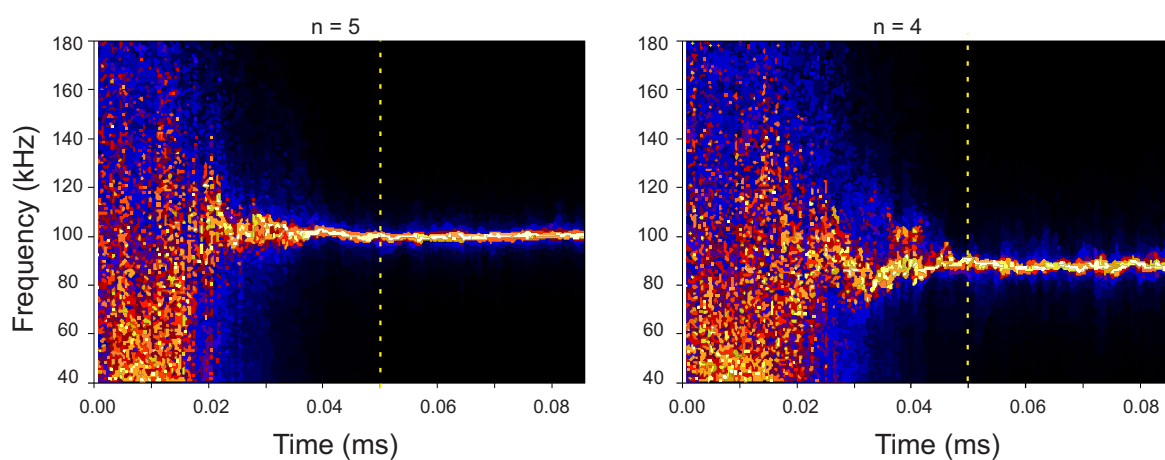


Fig. 4.8 The time evolution of the Fourier transform (in time) of the  $n$ -modes shows that  $n = 4, 5$  have a coherent frequency from 0.05 ms.

well as the energy that the  $n$ -modes increases (top figure of 4.3). This time window then becomes really important, since it can be seen in figure 4.6d, counter-going particles start being expelled. This coincidence in time may lead to the fact that these particles are being expelled by these instabilities.

# Chapter 5

## Conclusions and future work

During this work, a 3D wall for the ASDEX Upgrade tokamak has been included in the simulation model to study the simulated fast-ion losses during the plasma evolution. To accomplish this goal, the underlying physical, mathematical and numerical models of MEGA have been studied to have a global overview of the plasma physics and understand, from the theoretical point of view, the results obtained in the simulation. A particular type of instability has been studied, the *Toroidal Alfvén Eigenmode*, TAE. A possible TAE mode has been found in the simulations, having a well-defined frequency as it was theoretically predicted.

A first correlation between the plasma kinetic energy and the fast-ion losses rate at the wall has been observed. Moreover, a correlation between the TAE initial time and the place in the velocity space of the losses has been found.

The results obtained with the implementation of the wall are the basis for future studies of the impact of fast-ion losses in ASDEX Upgrade, that can partially reveal the behavior of the fast-ion losses when instabilities are present in the plasma.

Future work includes the finalization of the 3D wall implementation to obtain much more reliable results of the fast-ion losses, that can be compared to those obtained from other numerical models, such as ASCOT [22] or to experimental data from the Fast-Ion Loss Detectors (FIELD).

Part of this work has been presented in a contribution for the European Physical Society Conference 2018 in Prague [23].

# Nomenclature

## Acronyms / Abbreviations

AUG ASDEX Upgrade tokamak [Max Planck Institute for Plasma Physics, Garching]

DFT Discrete Fourier Transform

DIV Divertor

FILD Fast-ion loss detector

FLR Finite Larmor Radius

HFS High-Field Side

HM Hazeltine-Meiss MHD

LCFS Last Closed Flux-Surface, equivalent to separatrix

LFS Low-Field Side

MHD Magnetohydrodynamics

NBI Neutral Beam Injector

PDE Partial Differential Equation

PIC Particle in Cell

TAE Toroidal Alfvén eigenmode



# References

- [1] H.-S Bosch and G M Hale. Improved formulas for fusion cross-sections and thermal reactivities.
- [2] Y. Todo and T. Sato. Linear and nonlinear particle-magnetohydrodynamic simulations of the toroidal Alfvén eigenmode. *Phys. Plasmas*, 5(5):1321–1327, 1998.
- [3] M. García-Muñoz, H.-U. Fahrbach, H. Zohm, and the ASDEX Upgrade Team. Scintillator based detector for fast-ion losses induced by magnetohydrodynamic instabilities in the ASDEX upgrade tokamak. *Rev. Sci. Instrum.*, 80(5):053503, may 2009.
- [4] J. Ayllon-Guerola, J. Gonzalez-Martin, M. Garcia-Munoz, J. Rivero-Rodriguez, A. Herrmann, S. Vorbrugg, P. Leitenstern, S. Zoletnik, J. Galdon, J. Garcia Lopez, M. Rodriguez-Ramos, L. Sanchis-Sanchez, A. D. Dominguez, M. Kocan, J. P. Gunn, D. Garcia-Vallejo, and J. Dominguez. A fast feedback controlled magnetic drive for the ASDEX Upgrade fast-ion loss detectors. *Rev. Sci. Instrum.*, 87(11):11E705, nov 2016.
- [5] J. Gonzalez-Martin et al. First measurements of a scintillator based Fast-Ion Loss Detector near the ASDEX Upgrade divertor. *Rev. Sci. Instruments (accepted)*, 2018.
- [6] J Wesson. *Tokamaks*. Clarendon Press - Oxford, 2004.
- [7] Simon David Pinches. *Nonlinear Interaction of Fast Particles with Alfvén Waves in Tokamaks*. Number November. 1996.
- [8] G. Y. Fu and J. W. Van Dam. Excitation of the toroidicity-induced shear Alfvén eigenmode by fusion alpha particles in an ignited tokamak. *Phys. Fluids B*, 1(10):1949–1952, 1989.
- [9] G. Y. Fu and J. W. Van Dam. Stability of the global Alfvén eigenmode in the presence of fusion alpha particles in an ignited tokamak plasma. *Phys. Fluids B*, 1(12):2404–2413, 1989.
- [10] Y. Todo and T. Sato. Linear and nonlinear particle-magnetohydrodynamic simulations of the toroidal Alfvén eigenmode. *Phys. Plasmas*, 5(5):1321–1327, 1998.
- [11] Y. Todo, M. A. Van Zeeland, and W. W. Heidbrink. Fast ion profile stiffness due to the resonance overlap of multiple Alfvén eigenmodes. *Nucl. Fusion*, 56(11), 2016.

- 
- [12] Y. Hu, Y. Todo, Youbin Pei, Guoqiang Li, Jinping Qian, Nong Xiang, Deng Zhou, Qilong Ren, Juan Huang, and Liqing Xu. Simulation of fast-ion-driven Alfvén eigenmodes on the Experimental Advanced Superconducting Tokamak. *Phys. Plasmas*, 23(2), 2016.
- [13] Youbin Pei, Nong Xiang, Wei Shen, Youjun Hu, Y. Todo, Deng Zhou, and Juan Huang. Simulations of toroidal Alfvén eigenmode excited by fast ions on the Experimental Advanced Superconducting Tokamak Simulations of toroidal Alfvén eigenmode excited by fast ions on the Experimental Advanced Superconducting Tokamak. *Cit. Phys. Plasmas*, 25, 2018.
- [14] A. H. Boozer. Physics of magnetically confined plasmas. *Rev. Mod. Phys.*, 76(4):1071–1141, 2004.
- [15] A. Bock. *Generation and Analysis of Plasmas with Centrally Elevated Helicity Profiles in Full W ASDEX Upgrade*. PhD thesis, Ludwig-Maximilian University Munich, 2016.
- [16] E. Viezzer. Radial electric field studies in the plasma edge of ASDEX Upgrade. *PhD Thesis*, 2012.
- [17] Y. Todo, M. A. Van Zeeland, A. Bierwage, and W. W. Heidbrink. Multi-phase simulation of fast ion profile flattening due to Alfvén eigenmodes in a DIII-D experiment. *Nucl. Fusion*, 54(10), 2014.
- [18] A. Spitkovsky. Note on kinetic Plasma Simulations, Princeton.
- [19] Open-MPI.org. Open MPI: Open Source High Performance Computing, 2011.
- [20] J. Erickson. The Jordan Polygon Theorem. *Comput. Topol.*, pages 1–4, 2009.
- [21] Y. Todo, M. A. Van Zeeland, A. Bierwage, W. W. Heidbrink, and M. E. Austin. Validation of comprehensive magnetohydrodynamic hybrid simulations for Alfvén eigenmode induced energetic particle transport in DIII-D plasmas. *Nucl. Fusion*, 55(7), 2015.
- [22] Simppa Käslömpö, Taina Kurki-Suonio, Seppo Sipilä, and Ascot Group. Synthetic Fast Ion Diagnostics in Tokamaks: Comparing the Monte Carlo Test Particle Code ASCOT Against Experiments. 1055, 2017.
- [23] J. Gonzalez-Martin, M. Garcia-Munoz, Y. Todo, S.E. Sharapov, M. Dunne, V. Igochine, R. Fischer, P. Oyola, L. Sanchis-Sanchez, A. J., and E. Viezzer. Non-Linear 3d Hybrid Kinetic-MHD Simulations of Alfvén Eigenmodes in the ASDEX Upgrade Tokamak. 2018.

# Appendix A

## Theoretical plasma physics

### A.1 Eigenvalue equation for MHD instabilities

The eigenvalue equation for the MHD equations can be derived from the complete set of equations of the ideal MHD (2.7) - (2.12). The first step towards obtaining the eigenvalue equation is to linearize these equations. This can be done by considering that all the magnitudes can be decomposed into two terms  $A = A_0(\vec{r}) + A_1(\vec{r}, t)$ , where the subscript 0 corresponds to the equilibrium value, that may be inhomogeneous, and the subscript 1 is a perturbation over the equilibrium that can evolve in time. For linearization the ordering in the perturbation larger than the linear term is neglected (this is assuming that the perturbation is small enough).

The linearized system is:

$$\begin{aligned}\frac{\partial \rho_1}{\partial t} + \vec{\nabla} \cdot (\rho_0 \vec{v}_1) &= 0 \\ \frac{\partial p_1}{\partial t} + \vec{v}_1 \cdot \vec{\nabla} p_0 + \gamma p_0 \vec{\nabla} \cdot \vec{v}_1 &= 0\end{aligned}$$

$$\begin{aligned}\frac{\partial \vec{B}_1}{\partial t} &= \vec{\nabla} \times (\vec{v}_1 \times \vec{B}_0) \\ \mu_0 \vec{J}_1 &= \vec{\nabla} \times \vec{B}_1 \\ \rho_0 \frac{\partial \vec{v}_1}{\partial t} &= \vec{J}_1 \times \vec{B}_0 + \vec{J}_0 \times \vec{B}_1 - \vec{\nabla} p_1\end{aligned}$$

Integrating the previous set of equations in time, taking into account that  $\vec{\xi} = \frac{\partial \vec{\xi}}{\partial t}$ :

$$\rho_1 = -\vec{\nabla} \cdot (\rho_0 \vec{\xi}) \quad (\text{A.1})$$

$$p_1 = -\vec{\xi} \cdot \vec{\nabla} p_0 - \gamma p_0 \vec{\nabla} \cdot \vec{\xi} \quad (\text{A.2})$$

$$\vec{B}_1 = \vec{\nabla} \times (\vec{\xi} \times \vec{B}_0) \quad (\text{A.3})$$

$$\rho_0 \frac{\partial^2 \vec{\xi}}{\partial t^2} = \vec{F}(\vec{\xi}) \quad (\text{A.4})$$

If one now applies a Fourier transform in time, the previous equations become an a set of eigenvalue equations, that can be further simplified (as shown in [8] and [9]) by considering an angular decomposition and studying only the radial perturbation.

## A.2 Hazeltine-Meiss model: viscosity and energetic particles

The general form of the MHD equations is given in (2.2)-(2.4), but for further analysis more explicit expressions are needed.

### PRESSURE TENSOR

The pressure tensor can be decomposed into two terms:

$$\mathbf{P} = p\mathbf{1} + \tau$$

where  $p$  is the thermodynamical pressure and  $\tau$  stands for the Cauchy's stress tensor, related to the gradient in the velocity field of the fluid ( $\vec{\nabla}u$ ). A linear constitutive equation can be used as first approach:

$$\tau = \lambda(\vec{\nabla} \cdot \vec{u})\mathbf{1} + \mu(\vec{\nabla} \otimes \vec{u} + \vec{\nabla} \otimes \vec{u}^T)$$

where  $\lambda$  and  $\nu = \mu/\rho$  are the *bulk viscosity* and the *viscosity*, respectively. The tensor can be generally splitted into two terms, one containing the diagonal part and a traceless tensor, containing all the anisotropy of the system:

$$\tau = (\lambda + \frac{2}{3}\mu)(\vec{\nabla} \cdot \vec{u})\mathbf{1} + \mu(\vec{\nabla} \otimes \vec{u} + \vec{\nabla} \otimes \vec{u}^T - \frac{2}{3}(\vec{\nabla} \cdot \vec{u})\mathbf{1})$$

The divergence of the non-diagonal components of the pressure becomes:

$$\vec{\nabla} \cdot \tau = \vec{\nabla}(\zeta \vec{\nabla} \cdot \vec{u}) + \frac{1}{3}\vec{\nabla}(\vec{\nabla} \mu \vec{u}) \vec{\nabla}^2(\mu \vec{u})$$

where  $\zeta = \lambda + \frac{2}{3}\mu$  is introduced.

Using this expression and rearranging the terms in the momentum equation (using conveniently the vector relations of  $\vec{\nabla}$  operator):

$$\rho \frac{d\vec{u}}{dt} = -\vec{\nabla} \tilde{p} + \frac{4}{3}\vec{\nabla}(\rho \nu \vec{\nabla} \cdot \vec{u}) - \vec{\nabla} \times (\rho \nu \vec{\omega}) \quad (\text{A.5})$$

where:

- $d/dt$ , here stands for the **advective derivative**;
- $\tilde{p}$  is not the thermodynamical pressure, but a modification due to the general anisotropy in plasma:

$$\tilde{p} = p - \zeta \vec{\nabla} \cdot \vec{u}$$

It is usually assumed that the corrections to the thermodynamical pressure are negligible so  $\tilde{p} \approx p$ ;

- the vorticity of the fluid,  $\vec{\omega} = \vec{\nabla} \times \vec{v}$ , is also introduced as a natural term within the fluid mechanics;
- the momentum induced by the current and the magnetic field has been dropped for clarity.

Moreover, in the Hazeltine-Meiss model, more frictional terms are required. A quantitative description of such quantities requires the discussion of Fokker-Planck equations and other stochastic methods.

## ENERGETIC PARTICLES CURRENT COUPLING

The inclusion of the fast-ions in the plasma modelling requires taking into account the interaction between them and the bulk plasma. From the two-fluids equations:

$$\begin{aligned}\rho_b \frac{d\vec{v}_b}{dt} &= -\vec{\nabla} \cdot \mathbf{P}_b + \rho_b \vec{E} + \vec{J}_b \times \vec{B} \\ \rho_H \frac{d\vec{v}_{fi}}{dt} &= -\vec{\nabla} \cdot \mathbf{P}_\alpha + \rho_b \vec{E} + \vec{J}_\alpha \times \vec{B}\end{aligned}$$

where subindex  $b$  and  $\alpha$  states for bulk plasma and fast-ions, respectively. Some assumptions can be made to combine these two equations:

1. Fast-ion density is much smaller than bulk plasma:  $n_b \gg n_\alpha$ . Besides, their Larmor radius is larger than the typical one for bulk plasma, so the perpendicular component of the pressure contribution for EP can be neglected against bulk plasma;
2. Quasineutrality applies:  $\rho_b \approx 0$ ;
3. The rate of change in the fast-ion fluid velocity is negligible with respect to the bulk plasma.

Subtracting conveniently the previous expressions and applying the previous approximations:

$$\rho_b \frac{d\vec{v}_b}{dt} = -\vec{\nabla} \cdot \mathbf{P}_b - \rho_H \vec{E} + (\vec{J}_b - \vec{J}_\alpha) \times \vec{B}$$

Further simplifications can be made if one considers that the fast-ion current can be splitted into two terms,  $\vec{J}_\alpha = \vec{J}'_\alpha + \vec{J}_{E \times B}$ , where the second one is the current produced by the  $\vec{E} \times \vec{B}$ -drift in fast-ions. Introducing such a definition in the previous equation and considering the electric field parallel to the magnetic field as negligible:

$$\vec{J}_{E \times B} \times \vec{B} = \rho_H \left( \vec{E} - (\vec{E} \cdot \vec{u}_B) \vec{u}_B \right) \approx \rho_H \vec{E}$$

this reads to:

$$\rho_b \frac{d\vec{v}_b}{dt} = -\vec{\nabla} \cdot \mathbf{P}_b + (\vec{J}_b - \vec{J}'_\alpha) \times \vec{B} \quad (\text{A.6})$$

### A.3 Grad-Shafranov equation

In the ideal MHD, the equilibrium situation can be easily described using the force balanced equation:

$$\vec{J} \times \vec{B} = \vec{\nabla} \times \vec{B} \times \vec{B} = \vec{\nabla} p \quad (\text{A.7})$$

which explicitly establish the equilibrium between the magnetic force (left-hand side) and the pressure gradient (right-hand side), where  $\mu_0$  has been dropped for simplicity. The axisymmetry in a tokamak makes that the equilibrium is independent on the toroidal angle,  $\phi$ . In particular, it allows introducing a more convenient coordinate: the magnetic flux,  $\psi$ .

$$\vec{B} \cdot \vec{\nabla} \psi = 0 \quad (\text{A.8})$$

which can be splitted into two equations:

$$\begin{aligned} B_r &= -\frac{1}{r} \frac{\partial \psi}{\partial z} \\ B_z &= \frac{1}{r} \frac{\partial \psi}{\partial r} \end{aligned}$$

From (A.7) it is clear that there exists a symmetry between magnetic field and current density, a new flux is introduced:

$$\begin{aligned} j_r &= -\frac{1}{r} \frac{\partial f}{\partial z} \\ j_z &= \frac{1}{r} \frac{\partial f}{\partial r} \end{aligned}$$

Through the Ampere law, a relation between  $f = f(\psi)$  and magnetic can be derived:

$$f = \frac{r B_\phi}{\mu_0}$$

To derive the Grad-Shafranov equation, (A.7) can be rewritten in terms of poloidal current and magnetic field, which can be easily related to the magnetic flux:

$$-\frac{B_\phi}{r} \vec{\nabla} f + \frac{J_\phi}{r} \vec{\nabla} \psi = \vec{\nabla} p$$

Using chain rule (since all parameters depends on the magnetic flux) and considering the previously defined fluxes:

$$J_\phi = r p' + \frac{\mu_0}{r} f f'$$

where the derivatives are taken with respect to magnetic flux,  $\psi$ . Finally, using Ampere law and properly combining all these results, the Grad-Shafranov equation is obtained:

$$R \frac{\partial}{\partial R} \left( \frac{1}{R} \frac{\partial \psi}{\partial R} \right) + \frac{\partial^2 \psi}{\partial z^2} = -\mu_0 R^2 p'(\psi) - \mu_0^2 f(\psi) f'(\psi) \quad (\text{A.9})$$

where  $r$  has been changed to  $R$  in the final result.